Phosphines on Colloidal Nickel Nanocatalysts to Lower the Onset Temperature of Terminal Alkynes Hydrogenation

Karim Azouzi, Anthony Ropp, Sophie Carenco

Phosphines on Colloidal Nickel Nanocatalysts to Lower the Onset Temperature of Terminal Alkynes Hydrogenation

Karim Azouzi,[1] *Anthony Ropp,*[1] *Sophie Carenco,*[1,*]

[1] Sorbonne Université, CNRS, Laboratoire de Chimie de la Matière Condensée de Paris (LCMCP), 4 place Jussieu, 75005 Paris, France

E-mail: sophie.carenco@sorbonne-universite.fr

Abstract:

Catalysis by colloidal suspensions of metal nanoparticles (NPs) is becoming more and more attractive as it may combine mild reaction conditions with the use of organic ligands as surface modifiers. While most examples focus on increasing the selectivity of the catalytic process, there is also an opportunity to use the ligands to boost the conversion and to trigger the onset of activity at a temperature where the NPs alone would not be active. This may be achieved because the ligands modify the electronic and steric environment at the surface active site. In this work, we show that phosphines with adequate steric hindrance (e.g. P^nBu_3, P^iBu_3) lower the onset temperature for phenylacetylene hydrogenation by nickel NPs under 7 bar of H_2, by *ca* 10 to 20 °C depending on the NPs diameter. This result is not expected to have practical repercussion for the reaction at stake, as it is already well-mastered, yet it is of

conceptual value because the hydrogenation may have been driven by the frustrated Lewis pair (FLP) between the Lewis basic phosphine and the Lewis acid nickel surface, forming a so-called "NanoFLP". We investigated this proposal using 10 phosphines and used a stereo-electronic map to rationalize their ability to boost the conversion, showing that moderately hindered and fairly donating phosphines are most adequate. Moreover, we demonstrated that less than 2 phosphines per Ni surface atom are enough for the effect to arise. We showed that other terminal alkynes like 1-octyne can be hydrogenated with this method. Lastly, comparison of conversion for 5 *para*-substituted phenylacetylenes was used to discuss the effects of electronic donation and steric hindrance at the surface active site.

Keywords: alkynes, hydrogenation, nanocatalysis, nanoparticles, nickel, phosphine

1. Introduction

Catalysis with metal nanoparticles (NPs) was successfully developed in the context of heterogeneous catalysis, where the nanoparticles are typically deposited on a support. For example, nickel nanoparticles were used for a range of transformations such as methanation of CO_2,[1] CO_2 reforming of methane,[2] *N*-alkylation of amines,[3] selective hydrogenation of nitroarenes,[4] enantioselective hydrogenation of methyl acetoacetate,[5] etc. Notably, nickel NPs are a catalyst of choice for hydrogenation reactions, being less expensive than platinum-based catalysts.[6] However, while Pt nanoparticles may be active at room temperature, nickel nanoparticles require stronger operating conditions to be active, typically, above 100 °C and under more than 10 bars of H_2.[4,5]

Nowadays, there is a strong interest in developing nanocatalysts as colloidal suspensions,[7–9] targeting milder operating conditions, typically below 100 °C and with only a few bars of gas.[10] Under such conditions, two goals may be achieved. First, the reaction products may be

more fragile molecules, with a richer set of chemical moieties. Second, the selectivity of the reaction may be improved thanks to the lower activation energy provided to the reaction. Strategies to enhance the reactivity of metal nanocatalysts in colloidal suspensions include the use of non-classical solvents such as ionic liquids[11,12] or glycerol,[13] activation by external stimuli such as a magnetic field,[14] or a fine design of the metal-solution interface.[15] Within this last category, organic ligands that bind to the metal surface were employed, mostly for two purposes. The first was to poison the most active sites in order to enhance the reaction selectivity,[16] the second was to provide a chiral environment for the reaction and develop enantioselective nanocatalysis.[17]

Recently, it was proposed that Lewis base ligands may provide a new type of surface active site on NPs, to promote the reaction under mild conditions. The underlying idea was to transpose the concept of Frustrated Lewis Pairs (FLPs) to surfaces. FLPs are well-known in organocatalysis, where it was demonstrated that H_2 could be cleaved at 25 °C by the frustrated adduct $^{t}Bu_3P \rightarrow B(C_6F_5)_3$.[18] In the case of semi-heterogeneous FLPs, it is proposed to replace the Lewis acid borane by a metal nanoparticle surface, such as gold or nickel. When this acid surface belongs to a nanoparticle that is supported or suspended in solution, it freely interacts with the Lewis base ligand (such as a bulky enough amine or phosphine) that is present in the solution.

The pair made of the acid surface and the molecular base might be able to activate H_2 as efficiently as FLPs from organocatalysis. Strong successes were obtained with gold nanoparticles by the group of Rossi: while gold is typically not a good hydrogenation catalyst, the addition of nitrogen-containing Lewis base ligands such as amines allowed the hydrogenation of phenylacetylene and other alkynes at 80 °C under 6 bars of H_2.[19] A prior work by the group of Guo, mostly based on DFT modeling, had demonstrated that a frustrated

Lewis interaction on the gold surface was responsible for the unexpected activity of gold surface exposed to nitrogen-containing Lewis bases.[20] Phosphines are a family of Lewis bases that allows for a large tuning of electronic and steric parameters. This was exploited in the work by Cokoja *et al.*:[21] they demonstrated that phosphines may enhance the hydrogenation performances of Pd nanoparticles, although it was rationalized in relation to the electronic donation from the ligand to the metal surface. Besides, phosphine embedded into silica nanoreactors were shown to affect the catalytic activity of Ru and Pd nanoparticles.[22,23]

In our group, we are interested in exploring the concept of Frustrated Lewis Pairs built with phosphines and nanoparticles of transition metals, which are more abundant and thus more desirable than noble metals. In a first work, we suggested for another reaction, the hydrosilylation of benzaldehyde, that the surface of NiCo nanoparticles and phosphine ligands may be forming what we called a "NanoFLP", meaning a FLP at the surface of a nanoparticle in a colloidal suspension.[24,25] In this case, because a rich shell of ligands is present to insure the colloidal stability of the nanoparticles, we would expect that the steric hindrance at the surface, which opposes with the propensity of the ligand to bind, is partly responsible for the frustrated interaction.

Our objective in this article was to evaluate the possibility to form NanoFLP for hydrogenation reactions, using nickel nanoparticles. We expected that the pairing of nickel nanoparticles with well-chosen phosphine ligands, in a regime where their access to the surface would be frustrated by local steric hindrance and/or electronic repulsion (as shown for gold by the group of Guo),[26] may result in an increased activity for hydrogenation reactions. As an additional point, we also investigated the effect of the diameter of the Ni core on the catalytic behavior, because it influences the ratio of the Lewis base to the metal surface atom.

Well-calibrated nickel nanoparticles were available from a robust synthesis that required only three reactants, thus lowering the intrinsic complexity of the system.[27,28]

We found that the hydrogenation of phenylacetylene by size-controlled nickel nanoparticles (diameters of 18 nm, 11 nm, 23 nm) under 7 bars of H_2 was achieved at a lower temperature in the presence of some phosphines (*e.g.* P^nBu_3) than in their absence, while other phosphines (*e.g.* PPh_3) had no significant effect. This was rationalized based on a stereo-electronic map. Moreover, the phosphine stoichiometry had to be carefully tuned for the onset temperature to be lowered. This was observed regardless of the nanoparticle diameter, while the effect arose at a lower temperature for the larger ones (50, 60 and 80 °C for 23, 18 and 11 nm, respectively). Some *para*-substituted phenylacetylenes were also hydrogenated. Finally, we discussed the origin of the activity enhancement, in particular, whether it was due to a frustrated Lewis pair formed by the surface and the phosphine, which would have performed the heterolytic cleavage of H_2, or it was induced by a more distant modification of the surface electronic properties as a consequence of the phosphine coordination.

2. Results and discussion

2.1. Effect of P^nBu_3 on the hydrogenation of phenylacetylene by Ni NPs (18 nm diameter)

As a first step, we investigated the hydrogenation of phenylacetylene using spherical nickel nanoparticles of 18 nm average diameter as catalysts. The synthesis of the nanoparticles was reported elsewhere.[27,28] As schematized on Figure S1A, it consisted in the reduction of Ni(acetylacetonate)$_2$ by oleylamine at 220 °C, in the presence of tri-*n*-octylphosphine (TOP) as the main stabilizing ligand. Transmission electron microscopy (TEM) confirmed the morphology and diameter of the nanoparticles (Figure S1B). X-ray diffraction on powder

(XRD) confirmed that they were crystallized in the cubic phase (Figure S1C), with an average crystallite size of ca 4 nm, lower than the nanoparticle diameter, as expected from this synthetic path.[27]

Catalytic reaction without or with P^nBu_3 as Lewis base

These nanoparticles were dispersed to form a colloidal suspension in toluene and they were engaged in a hydrogenation reaction using H_2 (7 bar), in the attempt to study the efficiency of the H–H bond activation by the nanoparticle surface. Phenylacetylene was selected as a model substrate. The reactions were monitored by ^{1}H NMR and a typical spectrum is shown in Figure S2 (see Experimental section for details). The reaction was performed at 40, 50, 60 and 80 °C (Figure 1B, entries 1, 3, 5, 7) with a catalyst loading of 10 mol% (of Ni atoms *vs.* the phenylacetylene). No significant activity was observed below 80 °C (Figure 1C, grey triangles), while the conversion reached 100 %, with a selectivity of 46 % for styrene, at 80 °C (Figure 1B, entry 7).

The same reaction was then investigated in the presence of an additional molecule, the Lewis basic phosphine P^nBu_3 (0.2 equiv., *i.e.* 20 mol%, *vs.* phenylacetylene). First, it should be noted that the blank reaction, with the phosphine but without Ni NPs, yielded no conversion at 60 °C and traces of styrene (2 %) at 100 °C, discarding a catalytic activity of the Lewis base alone in the temperature range 40 – 80 °C.

In the presence of Ni NPs, while there was no conversion at 40 °C, a significant conversion was achieved at 50 °C with a selectivity of 87 % for styrene (Figure 1B, entries 2 and 4, respectively). At 60 °C, a quantitative conversion was reached with a selectivity of 44 % for styrene (Figure 1B, entry 6). At a higher temperature of 80 °C, the conversion was still quantitative but the selectivity was lower (Figure 1B, entry 8). By comparison, the nanoparticles catalytic activity was thus boosted by the presence of P^nBu_3 at the intermediate

temperature of 50 °C (Figure 1C, red circles). Besides, the fairly poor selectivity of these nickel catalysts was confirmed, as expected from a previous work.[29] Optimizing the selectivity is however not the aim of the present work, which is primarily focused on the activation of H_2 by the nanoparticle-phosphine pair. However, it should be noted that decreasing the H_2 pressure improved the selectivity of the reaction (Table S4). Styrene was formed at 87 % under 3 bar (entry 2) and was the sole product under 1 bar (entry 3). This was unfortunately accompanied by a decreased conversion of 97 and 10 %, at 3 and 1 bar respectively.

A

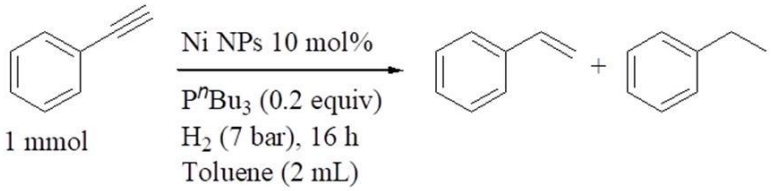

B

Entry	T (°C)	Lewis Base	Phenylacetylene conversion (%)	Styrene / Ethylbenzene
1	40	-	0	-
2	40	P^{n}Bu$_3$	0	-
3	50	-	3	>99/0
4	50	P^{n}Bu$_3$	47	87/13
5	60	-	0	-
6	60	P^{n}Bu$_3$	>99	44/56
7	80	-	>99	46/54
8	80	P^{n}Bu$_3$	>99	30/70

C

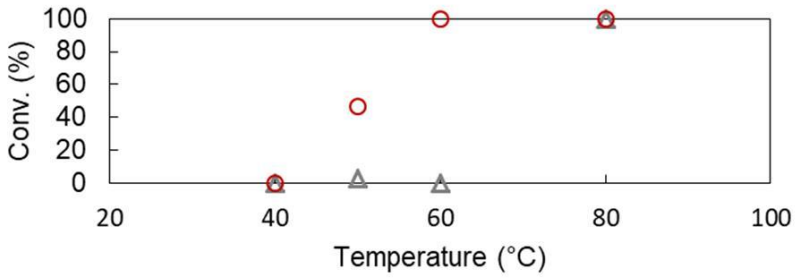

Figure 1. Influence of the temperature on the catalytic activity of Ni (18 nm) NPs with and without phosphine. (A) Reaction scheme. Reaction conditions: phenylacetylene (110 µL, 1 mmol, 1 equiv.), Ni NPs (0.1 mmol, 0.1 equiv. of Ni atoms), P^{n}Bu$_3$ (0.2 mmol, 0.2 equiv.), toluene (2 mL), 16 h, H_2

(7 bar). Optimized conditions correspond to 60 °C. (B) Catalytic results. (C) Graphical representation of (B).

At this stage, we postulated a synergy of the phosphine with the nickel surface during the hydrogenation of phenylacetylene, but the first point to verify was the heterogeneous nature of the catalysis. For this purpose, the nanoparticles were characterized *post-mortem* and a leaching test was used.

Post-mortem analysis

The spent nanoparticles were observed by TEM (Figure S3). No significant change in average size was observed *vs.* the fresh nanoparticles. The surface of the nanoparticles was also characterized using X-Ray Photoelectron Spectroscopy (XPS). The signal/noise ratio was fairly low, which prevented a full fit of the data, but these were interpreted in comparison with a previous work.[24] Small changes were observed as a consequence of the catalytic reaction. First, the nickel was slightly more reduced after the reaction, as indicated by the growth of the signal at binding energy (B.E.) 852–853 eV. This is an expected consequence of prolonged exposure to H_2. On the other hand, the presence of nickel oxidized species, visible through the satellite peak at B.E. 855–857 eV, was explained by their washing under air. Second, the P 2p region indicated a higher proportion of oxidized P species, as indicated by a relative increase of the $P^{(+V)}$ species in the region 132–134 eV. We related this to oxidation of the phosphines after exposure to air of the spent catalyst.

Moreover, in order to know the state of the phosphine after the reaction in air-free conditions, $^{31}P\{^{1}H\}$ NMR of the supernatant was performed (Figure S4A) using a larger amount of $P^{n}Bu_3$ (1 equiv.) to be well over the detection limit. It should be reminded that solution NMR mostly detects the molecules in the solution, rather than those coordinated to the surface of the nanoparticles. $P^{n}Bu_3$ was observed as the main species at -32.3 ppm and a few other species

were detected only as traces, at 42.7, 36.3 and 33.4 ppm. The first was attributed to $O=P^nBu_3$ and the others were not identified. As a side-note, it should be noted that the two unidentified species would also form when performing the experiment in the absence of Ni NPs, while no conversion was observed (Figure S4Bb). A complementary experiment was also performed using a pressurized NMR tube, however this did not allow the identification of additional species (see SI, section 14).

This first set of data confirmed that the nanocatalyst and the phosphine ligand survived the catalytic reaction. In order to eliminate the possible formation of catalytically active leached species, a leaching test was performed. It consisted in testing the activity of the supernatant a few hours after the catalytic reaction was started. Practically, the reaction was first performed for 6 h at 60 °C under 7 bars of H_2, in the presence of the nanoparticles and the phosphine (Scheme S1). A conversion of 18 % was obtained, indicating that the catalytic process was ongoing. Then, the reaction mixture was centrifuged and the nanoparticles were removed. The supernatant was submitted again to 7 bars of H_2 at 60 °C for 6 h. No further conversion was found, indicating that no catalyst was present in the supernatant.

At this point, we were able to confirm the heterogeneous nature of the catalysis. The role of the phosphine needed to be clarified. In this purpose, several phosphines were tested. Our working hypothesis was that the presence of a phosphine keen to interact with the surface would lower the activation energy of the hydrogenation process, thus, allow the conversion of phenylacetylene at a lower temperature.

2.2. Influence of the phosphine basicity and steric hindrance on the Ni NPs catalytic activity

A screening of 9 phosphines was performed to investigate if the positive effect found for

P^nBu_3 could be identified for other ones. We selected the temperature of 60 °C, at which the presence of P^nBu_3 was necessary for the nanocatalyst to be active. The results in terms of conversion and styrene selectivity are shown in Table 1. With PPh_3 and $P(OPh)_3$, no improvement was observed *vs.* the reaction without phosphine, meaning that no conversion was observed (entries 5, 10 and 1, respectively). For all other phosphines, a positive effect was found, which we will discuss in detail. The selectivity was fairly high, above 80 % when the conversion was lower than 70 %, e.g. the selectivity was 85 % when using PCy_3. Our discussion will focus on the conversion.

For the butyl-phosphine family, with a conversion of 49 %, P^tBu_3 was less favourable than P^iBu_3 and P^nBu_3, which provided a quantitative conversion (entries 4, 3 and 2, respectively) in the presence of Ni NPs. Then, in the series $PMe_pPh_{(3-p)}$, with p from 0 to 3, the conversion was higher for p = 1 (PMe_2Ph, 53 %, entry 7) and decrease on each side (entries 5, 6 and 8), in the presence of Ni NPs. The results of both series were consistent with the idea that a compromise has to be found between the steric hindrance and the Lewis basicity of the phosphine.

Table 1. Phosphine screening: phenylacetylene conversion and selectivity for styrene. Reaction conditions: phenylacetylene (110 µL, 1 mmol, 1 equiv.), Ni (18 nm) (0.1 mmol, 0.1 equiv.), phosphine (0.2 mmol, 0.2 equiv.), toluene (2 mL), 60 °C, 16 h, H_2 (7 bar).

Entry	Phosphine	Phenylacetylene conversion (%)	Styrene/Ethylbenzene
1	-	0	-
2	P^nBu_3	>99	44/56
3	P^iBu_3	>99	83/17
4	P^tBu_3	49	92/8
5	PPh_3	0	-
6	$PMePh_2$	36	92/8
7	PMe_2Ph	53	96/4
8	PMe_3	19	95/5
9	PCy_3	70	85/15
10	$P(OPh)_3$	0	-
11	$P(OBu)_3$	13	85/15

In order to rationalize this first set of results, the phosphines were positioned on a stereo-electronic map, presented in a previous work.[30] This is a two-dimensional space based on the phosphine Tolman Electronic Parameter (TEP)[31] and on a steric hindrance parameter, for which we selected the free ligand descriptor He_8_steric developed for phosphorus donor ligands.[32,33] The map was color-coded, with lighter colors representing a higher conversion (Figure 2). It appeared that phosphines with a TEP close to 2060 cm^{-1} (P^nBu_3 and P^iBu_3), and a moderate steric hindrance, were the most favorable to trigger the catalytic activity of the nickel NPs at 60 °C.

In order to complete these findings, additional phosphines were tested. With a lower TEP of 2056.4 cm^{-1} but a steric hindrance between these of P^nBu_3 and P^iBu_3, PCy_3 appeared to provide a slightly less efficient enhancement of the conversion (70 %). On the side of higher

TEP, $P(O^nBu)_3$ allowed a modest conversion of 13 %, although its steric hindrance was very close to these of P^nBu_3.

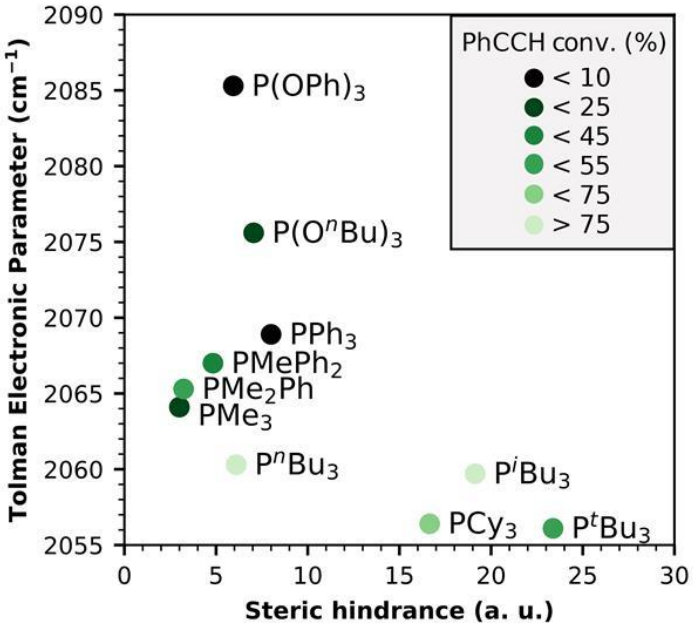

Figure 2. Stereo-electronic map of the phosphines. The color code for the conversion of phenylacetylene is indicated in the top right corner of the figure.

Altogether, the stereo-electronic map allowed delineating a region for which the enhancement was stronger, corresponding to TEP around 2060 cm^{-1} and intermediate steric hindrance. So far, a fairly large amount of phosphine was used (0.2 equiv.) in order to favor its interaction with the nanoparticle surface. Next, we investigated what would be the minimal number of ligands for the enhancement to take place.

2.3. Influence of phosphine stoichiometry

At this point, it should be reminded that the nickel nanoparticles were prepared in the presence of a long-chain alkylphosphine, the tri-*n*-octylphosphine, as a ligand limiting their growth. Because the nanoparticles were washed several times after synthesis, a limited number of these molecules remained available for the catalytic reaction. In contrast, when we

added 0.2 equiv. (*vs.* the phenylacetylene) of a new phosphine as done above, this phosphine was in large excess *vs.* the surface nickel atoms of the nanoparticles. Based on a geometric estimation, there were about 20 phosphines in total, per surface Ni atoms, meaning that a large proportion was solvated in the solution, free to come and go from the surface vicinity (see Table S2 entry 6 and SI section 7 for details of the calculation). We thus varied the stoichiometry of the phosphine in order to get insights into its role, using P^nBu_3 as a model compound. As shown in Figure 3A, 0.01 equiv. of P^nBu_3 was not enough to trigger the catalytic activity of the Ni NPs (Figure 3A, entry 1), and this value roughly corresponds to one phosphine per surface Ni atom (Table S2 entry 2). This might be indicative of the existence of a threshold in terms of phosphine concentration, as recently found for CoP nano-urchins.[34] However, a conversion of 81 % was observed with 0.025 equiv. (Figure 3A, entry 3), corresponding to a ratio of phosphine to Ni surface atom of ca 2.4 (Table S2 entry 3). Higher amounts of phosphine led to a quantitative conversion (Figure 3A, entries 4–7) with a declining selectivity, from 83 % for 0.05 equiv. to 41 % for 0.5 equiv. In these reaction conditions, the phosphine had to be introduced in excess *vs.* the surface Ni atoms for the catalytic activity to be observed (Figure 3B).

At this point, we decided to validate the two concepts identified so far using Ni NPs with smaller and larger diameters: *(i)* the existence of a temperature domain where the presence of the phosphine is critical to trigger the catalytic activity of the nanoparticles and, *(ii)* the strong influence of phosphine substoichiometric amounts (*vs.* the total number of nickel atoms) on the catalytic activity.

A

Entry	P^nBu_3 stoichiometry (equiv.)	Phenylacetylene conversion (%)	Styrene / Ethylbenzene
1	0	0	-
2	0.01	0	-
3	0.025	81	86/14
4	0.05	>99	83/17
5	0.1	>99	47/53
6	0.2	>99	44/56
7	0.5	>99	41/59

B

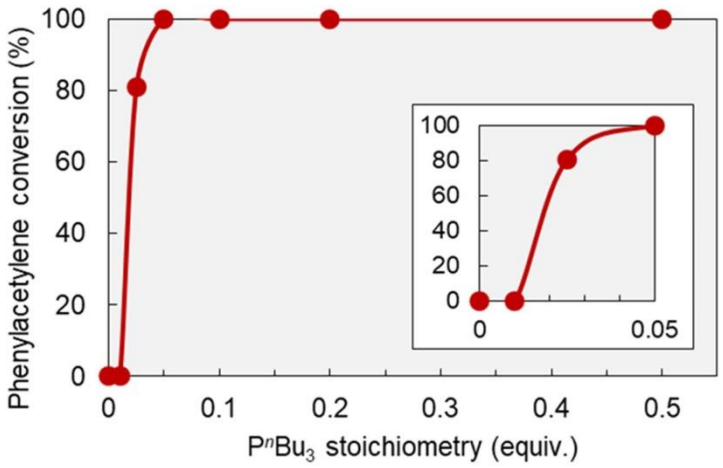

Figure 3. Effect of P^nBu_3 stoichiometry on the catalytic activity of Ni NPs (18 nm diameter). (A) Phenylacetylene conversion and selectivity for styrene. (B) Conversion *vs.* stoichiometry (inset: zoom on the 0-0.05 equiv. domain). The red line is a guide to the eye. Reaction conditions: phenylacetylene (110 µL, 1 mmol, 1 equiv.), Ni (18 nm) (0.1 mmol, 0.1 equiv.), toluene (2 mL), 60 °C, 16 h, H_2 (7 bar).

2.4. Influence of the Ni NPs diameter on their catalytic activity

In this purpose, NPs of 11 nm and 23 nm average diameter were prepared following a reported protocol, similar to that used for the 18 nm NPs (see SI section 3). Their round-shape morphology and average size were confirmed by TEM (Figure S5). As expected from this synthetic procedure, the smaller nanoparticles were poorly crystallized, as confirmed by HRTEM (Figure S6A, B), selected area diffraction (SAED) (Figure S7A) and XRD (Figure S8). In contrast with this, 23 nm diameter NPs were still polycrystalline, like the 18 nm NPs, but they exhibited a slightly larger average crystallite size of 6 nm (Figure S8)

and brighter diffraction spots in SAED (Figure S7C). By EDS, average P/Ni ratio of 0.18, 0.30 and 0.45 were found for 23, 18 and 11 nm NPs, respectively (see SI section 13).

For the purpose of comparing catalytic activity, it is also relevant to compare their surface state. XPS was performed on the NPs and the Ni 2p and P 2p regions are shown in Figure S9. As for the 18 nm NPs, the washing step in air was responsible for partial surface oxidation, and the use of TOP leads to some surface phosphidation, indicated by the P $2p_{3/2}$ peak at B.E. 129.1 eV. Altogether, the 11 nm and 23 nm NPs exhibit a surface state similar to these of the 18 nm NPs, allowing their comparison as nanocatalysts.

We then investigated the influence of P^nBu_3 (20 mol%) on the onset of catalytic activity for the NPs at temperatures from 40 to 80 °C. It should be noted that this onset is related to a given concentration of catalyst and a givent sensitivity for detecting the products, so all the further comments will be valid for the current set of experimental conditions. The results are reported in Table 2 and may be compared with these of Figure 1B. Interestingly, in the absence of phosphine, the smaller nanoparticles showed no activity in this temperature range (entries 1, 3, 5) while the larger ones were not active at 40 °C (entry 9) but provided a conversion of 11 % at 50 °C (entry 11).

Nevertheless, the positive effect of the phosphine could still be found in the lower temperature range in both cases. For the 11 nm Ni NPs, the phosphine triggered a full conversion at 80 °C (entry 6), with a moderate selectivity of 41 %. For the 23 nm Ni NPs, the phosphine had a significant effect already at 40 °C, by providing a conversion of 22 % (entry 10). Besides, as expected in the case of quantitative conversions, the selectivity for styrene was generally higher when a lower temperature was used (entries 10, 12, 14, 16). Data for the 18 nm Ni NPs were presented above, in Figure 1B.

Table 2. Influence of the reaction temperature on the hydrogenation of phenylacetylene with and without phosphine. Reaction conditions: phenylacetylene (110 µL, 1 mmol), Ni NPs (0.1 mmol of Ni, 0.1 equiv.), toluene (2 mL), 16 h, H_2 (7 bar).

Ni NPs diameter (nm)	Entry	T (°C)	P^nBu_3 (equiv.)	Phenylacetylene conversion (%)	Styrene / Ethylbenzene
11	**1**	40	0	0	-
	2		0.2	0	-
	3	60	0	0	-
	4		0.2	0	-
	5	**80**	**0**	**0**	-
	6		**0.2**	**>99**	**41/59**
	7	100	0	>99	67/33
	8		0.2	>99	16/84
23	**9**	**40**	**0**	**0**	-
	10		**0.2**	**22**	**100/0**
	11	50	0	11	83/17
	12		0.2	>99	62/38
	13	60	0	23	80/20
	14		0.2	>99	31/69
	15	80	0	>99	0
	16		0.2	>99	1/99

For the three sizes of nanoparticles, the onset temperature at which some conversion was observed was lower in the presence of phosphine than without. These experiments allowed us to define a critical temperature T_c, the highest temperature at which the nanocatalyst is active in the presence of the phosphine and inactive without. Our experiments were performed with steps of 20 °C, thus they only provide an estimate. The experimental values for T_c, marked in bold in Table 2, are respectively 80 °C, 60 °C and 40 °C for NPs with average diameters 11, 18 and 23 nm.

So far, the nanoparticles were compared at a constant amount of Ni atoms, meaning that the amount of surface Ni atoms significantly varied from one diameter to the other. Based on a geometric model (see SI section 7), the 11 nm Ni NPs have roughly 16 % of their atoms at the surface, while the 23 nm Ni NPs only have 8 % (Table S1). There are potentially twice more

Ni active sites for the smaller NPs than for the larger ones. The observed trend that larger nanoparticles were active at a lower temperature, despite a lower amount of Ni surface sites, may appear as counter-intuitive and will be discussed in section 2.6.

Moreover, the estimated stoichiometric ratio of phosphine *vs.* surface Ni atoms was also affected by the NP diameter (Table S2). Larger nanoparticles encountered a larger excess of phosphine, from the viewpoint of their surface atoms. For example, for 0.2 equiv. of P^nBu_3, the ratio of phosphine to surface Ni atoms was 12.5, 20.0 and 24.6 for respectively 11 nm, 18 nm and 23 nm NPs.

Because the phosphine stoichiometry was found to be key to triggering the catalytic activity of the 18 nm NPs, we decided to further investigate it for the two other sizes. The experiments were done at T_c for each diameter. Data are shown in Tables S3 and S4, respectively. The conversion was plotted *vs.* the ratio of phosphine to surface Ni atoms and compared with these of 18 nm Ni NPs (Figure 4).

The general trends were the same for the three NPs size: a sharp increase in conversion with comparatively low amounts of phosphines. More precisely, less than 2 equiv. of P^nBu_3 *vs*. surface Ni atoms were required to boost the catalytic activity of the NPs. For 11 nm NPs, the enhancement effect was observed at 80 °C, with a conversion of 79 % in the presence of 0.3 phosphine/surface Ni atoms (0.005 equiv. *vs* the total amount of Ni atoms) (Table S3). It was observed at 50 °C for the 23 nm NPs, with a jump of conversion from 11 to 71 % as a consequence of the addition of 1.2 phosphine/surface Ni atoms (0.01 equiv. *vs* the total amount of Ni atoms) (Table S4). At this stage, we are unable to interpret the fact that the curves steepness vary with the nanoparticle diameter. Besides, in the regime where the phosphine was in large excess (up to ca 25 *vs.* the surface Ni atoms), no decrease in

phenylacetylene conversion was observed, suggesting that the substrate easily accesses the nickel surface despite the presence of the phosphine. Out of the scope of the present study, further experiments with 1-*d*-phenylacetylene might allow to investigate a possible the kinetic isotope effect related to phenylacetylene chemisorption.

Besides, a complementary comparison at shorter reaction times was performed at 80 °C (Table S7), and estimated values for TOF were calculated for the formation of styrene, while the selectivity was still 100 %. Methodological limitations however preclude us from comparing these data with the literature, for two reasons. First, an induction period was observed for the reaction, which we discuss later on. Second, under these conditions the reaction time selected were partly arbitrary, so the values provided are only accurate for semi-quantitative comparison within our study. Two TOFs were calculated (Table S8): not normalized (per number of total Ni atom), or normalized per number of surface Ni atoms. The two series of values were increasing with increasing NPs diameter, e.g. from 8.00 to 23.33 mmol/h/mmol $Ni_{surface}$ for NPs of respectively 18 and 23 nm.

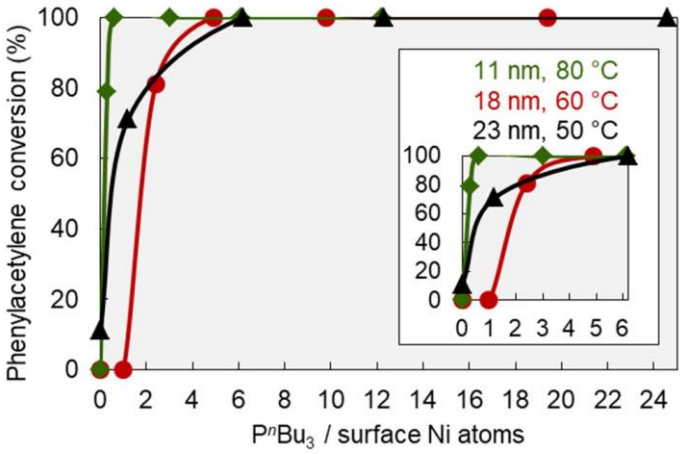

Figure 4. Phenylacetylene conversion by Ni NPs with diameters of 11, 18 and 23 nm. Reaction conditions: phenylacetylene (110 µL, 1 mmol, 1 equiv.), Ni NPs (0.1 mmol, 0.1 equiv.), toluene (2 mL), 16 h, H_2 (7 bar). Inset: legend and zoom on the 0 – 3 range. Lines are guides to the eye.

Altogether, this series of experiments confirmed that the conversion was strongly improved by the addition of phosphines, regardless of the NPs average diameter. The critical temperature for this effect was related to this diameter, with a higher temperature required for smaller nanoparticles. This phosphine effect was observed on top of the fact that the activity of the nanoparticles, prior to the addition of the phosphine, was observed at a lower temperature for the larger nanoparticles. In order to further investigate the role of the phosphine, the hydrogenation of *para*-substituted phenylacetylenes was investigated.

2.5. Hydrogenation of *para*-substituted phenylacetylenes

Variation of electronic and steric proprieties of the alkyne

For these experiments, 18 nm Ni NPs were used and a temperature of 50 °C was selected, in order to compare *para*-substituted phenylacetylene at conversion rates below 100 %. For five substituted alkynes, we investigated the influence of the presence of 0.2 equiv. P^{n}Bu$_3$ (Table 3). The table was ordered according to their Hammett parameter for *para*-substituents, which is 0 for phenylacetylene (entry 5) and varies from -0.27 to 0.54 for the other alkynes.[35] The

substitution in the *para* position was expected to have a limited effect on the steric hindrance at the alkyne moiety while it should have a strong effect on its electronic properties.

The conversion was not significant for 4-fluorophenylacetylene (entries 7 and 8) and 4-methoxyphenylacetylene (entries 1 and 2), regardless of the presence of the phosphine. For the three other alkynes, 4-methylphenylacetylene, 4-(trifluoromethyl)phenylacetylene and 4-bromophenylacetylene, conversions of respectively 11, 16 and 21 % were obtained in the presence of the phosphine, while the conversion was not significant in its absence (entries 3&4, 11&12 and 9&10, respectively). The phosphine thus enhanced the NPs activity for these three substrates, although the conversions were lower than for phenylacetylene (entry 6). Besides, these reactions with a limited conversion allowed a high selectivity for the alkene.

Overall, no clear trend was identified between the conversion and the Hammett parameter of the alkyne *para*-substituent. We believe that a further mechanistic investigation should include both electronic and steric effects in order to provide a clearer view of the reaction path. In particular, weak interactions (van der Waals or other) between the substituent and the ligands shell that surrounds the nanoparticle core may play a significant role when the alkyne approaches the nanoparticle surface. In order to further investigate this point, few terminal and internal alkynes were selected and studied.

Table 3. Influence of the *para*-substituent in phenylacetylene derivatives. Reaction conditions: Ni NPs (18 nm diameter, 0.1 mmol, 0.1 equiv.), P^nBu_3 (0.2 mmol, 0.2 equiv.), substrate (1 mmol, 1 equiv.), toluene (2 mL), 50 °C, 16 h, H_2 (7 bar).

Entry	Substrate	Hammett parameter	P^nBu_3 (equiv.)	Substrate conversion (%)	Alkene / Alkane
1	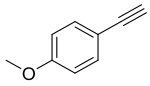	-0.27	0	0	-
2			0.2	2	100/0
3	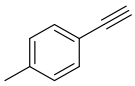	-0.17	0	2	100/0
4			0.2	11	100/0
5	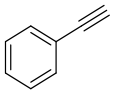	0	0	3	100/0
6			0.2	47	87/13
7	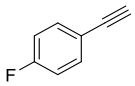	0.06	0	0	-
8			0.2	3	100/0
9	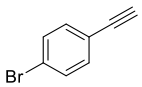	0.23	0	0	-
10			0.2	21	100/0
11	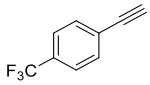	0.54	0	0	-
12			0.2	16	100/0

2.6. Hydrogenation of terminal *vs.* internal alkynes

Terminal alkynes are known to be easier to hydrogenate than internal ones. This is due in part to the acidity of the terminal hydrogen, and also in part to the lower steric hindrance of the carbon-carbon triple bond. We selected Ni nanoparticles (18 nm) and P^nBu_3 (0.2 equiv.) to evaluate this point under optimized conditions (60 °C, 16 h), under which no conversion was observed in the absence of the phosphine. The results are shown in Table 4. The hydrogenation of 1-hexyne, 1-octyne and 2-methyl-3-butyn-2-ol (entries 2 to 4) was quantitative in the presence of the phosphine, like these of the reference (phenylacetylene, entry 1). The selectivity was of the same order except for 2-methyl-3-butyn-2-ol where it was significantly lower (entry 4). In contrast with these results, internal alkynes such as diphenylacetylene, 3-hexyne, 2-hexyne, 4-octyne, 2-butyne-1,4-diol and dimethyl

acetylenedicarboxylate, were not hydrogenated under these reaction conditions (entries 5 to 10).

Table 4. Hydrogenation of terminal and internal alkynes. Reaction conditions: Ni NPs (18 nm diameter, 0.1 mmol, 0.1 equiv.), P^nBu_3 (0.2 mmol, 0.2 equiv.), substrate (1 mmol, 1 equiv.), toluene (2 mL), 60 °C, 16 h, H_2 (7 bar).

Entry	Substrate	Substrate conversion (%)	Alkene/Alkane (%)
1		>99	44/56
2	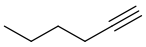	>99	45/55
3	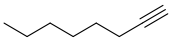	>99	60/40
4		>99	10/90
5		0	-
6	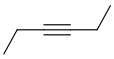	0	-
7	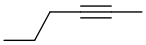	0	-
8	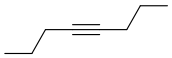	0	-
9	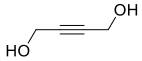	0	-
10	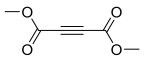	0	-

It is possible that the steric hindrance of diphenylacetylene prevents its approach to the surface. This hypothesis is consistent with the fact that the hydrogenation of phenylacetylene in the presence of diphenylacetylene, proceeds with a full conversion and a similar selectivity (competitive reaction, see SI section 10). However, the other internal alkynes tested here were not converted either. Future studies, possibly employing a less hindered phosphine, would be required to determine if appropriated reaction conditions may overcome the present limitation.

2.7. Discussion

This ensemble of results calls for a number of considerations. First, it should be reminded that the purpose of the work was not to improve, in general, the efficiency and selectivity of existing hydrogenation catalysts for the conversion of alkynes. Indeed, this reaction was already mastered with heterogeneous,[36] homogeneous and colloidal catalysts[37] through a number of works. Consistently with other works with Pd/C[38] and Pd nanoparticles,[21] the reaction was generally less selective for the alkene at higher conversions and higher H_2 pressure, due to the possibility to further hydrogenate the newly-formed alkene into alkane. This is related to the relative adsorption energies of alkene and alkynes at the surface of the NPs, depending on their coverage with ligands and/or hydride species. Moreover, Shevchenko *et al.* showed that a stronger adsorption energy for ligands *vs.* these of the alkene lowered the alkene hydrogenation, while high ligand coverage lowered the binding energy of the alkene on $CoPt_3$ NPs.[39] Here, our objective was rather to delineate the opportunity to form a NanoFLP using nickel NPs and phosphines. This is why we scrutinized the phenylacetylene conversion, rather than the styrene yield. Yet, we can still make a couple of general considerations about the selectivity. In our batch reactions, the selectivity for styrene could be only moderate when the conversion of phenylacetylene was full, meaning that the styrene was hydrogenated in a second step. At half conversion (with PMe_2Ph and P^tBu_3), the selectivity for styrene was very close, between 92 and 96 %. For reactions conducted with conversion of 70 % or less, the selectivity was higher than 92 % except for two phosphines: PCy_3 and $P(OBu)_3$ where the selectivity was 85 %. These are associated with conversions of 70 and 13 %, respectively, so we cannot provide a single explanation that would fit to both phosphines at this stage.

Regarding conversion, three parameters were varied in the purpose of clarifying the nature of the phosphine/NPs synergy: (i) the NPs average diameter, (ii) the phosphine steric and electronic properties and (iii) the electronic properties of the alkyne moiety. Prior to considering the phosphine, one should note that the onset temperature for the Ni NPs to show a catalytic activity decreased when increasing the diameter, for the three samples considered (Figure 5A, blue circles). This result suggests that the activation energy of the limiting step was lower when larger NPs were used. This result may appear as counter-intuitive but has a number of precedents. For example, for the hydrogenation of CO, the activation energy was found to be lower on large Co NPs (15 nm average diameter) than on smaller ones (4 nm average diameter).[40] Here, we wanted to relate this observation to the nature and spatial extension of facets. However, despite the round shape of the NPs, the crystallites are irregular in shape and poorly facetted, and our HRTEM data (Figure S6) does not allow such consideration. One may also keep in mind that, due to the synthetic process, the Ni surface is contaminated by phosphide species, which were found to be present at a higher rate for smaller NPs, as expected from the literature.[41,42] In the present case, XPS data did not allow discriminating this effect, and chemical analysis would not be precise enough due to the presence of phosphine as a native surface ligand.[43] Besides, it is reminded that the surface of Ni nanoparticles, as well as these of P-contaminated Ni nanoparticles, is able to achieve hydrogen-deuterium scrambling at a temperature as low as 25 °C, indicating that H–H bond cleavage can be performed on these surfaces.[44] In fact, preliminary data indicated that 9.5 nm crystalline Ni_2P nanoparticles were active for phenylacetylene hydrogenation at 60 °C in the presence of P^nBu_3, which we will discuss in due time in a separated report.

Thus, we move on and consider the effect of a phosphine such as P^nBu_3 on the onset temperature of catalytic activity. For all diameters considered, this phosphine allowed to

lower the temperature at which the Ni NPs catalyst was active, suggesting a synergy between the NPs surface and the ligand. Our attempts to measure an activation energy were hampered by several factors. First, the reactions show an induction time of a few hours, which we attribute to two possible phenomena: (i) the need to reduce the nickel oxide species that are at the surface of the nanoparticles as a result of washing in air, (ii) contact time required between the nanoparticles, the phosphine and/or the phenylacetylene for the active site to be generated. Second, once this induction time passed, the conversion would rapidly reach 100 %, meaning the reaction was slowed down by a lack of reactant, while a better analysis would have to be done at limited conversion. A flow setup, where conversion could be measured in-line, would be more suitable for a full kinetic analysis in future works.

Rather, and in order to advance the discussion of diameter effect, we defined above a critical temperature, T_c, at which the nanocatalysts is active in the presence of the phosphine and inactive without. T_c was plotted as a function of NPs diameter as green diamonds in Figure 5A. This temperature was lower for larger nanoparticles, following the trend observed before in the absence of phosphine. It should be noted that the temperature range for this effect is narrow, which may be why it was overlooked so far.

More importantly, the existence of the critical temperature indicates that the couple Ni NP/P^{n}Bu$_3$ performs the hydrogenation reaction with a lower activation energy than the Ni NP alone. This is in our opinion the main finding of this article. It would be consistent with the idea of Ni NPs and P^{n}Bu$_3$ forming a NanoFLP, into which H_2 and/or the phenylacetylene would be more easily activated than on the native surface of the NPs, which will now be discussed in detail.

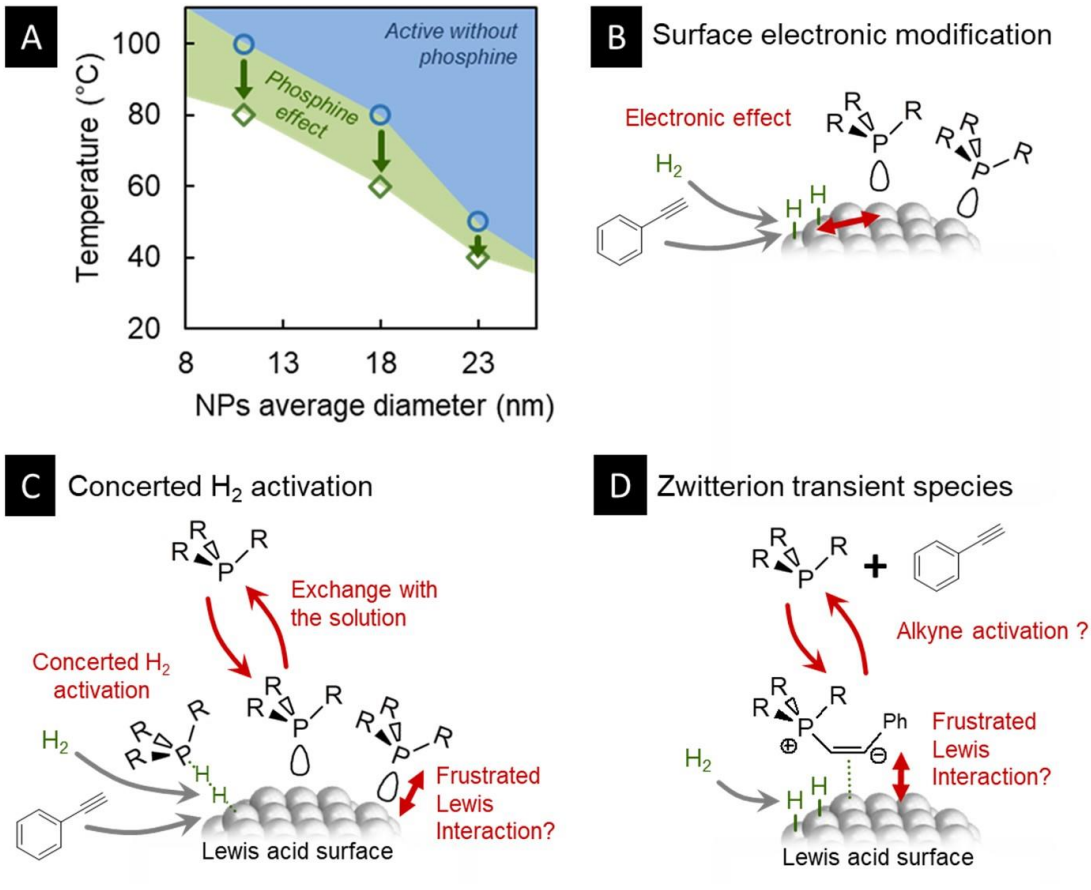

Figure 5. (A) Green diamonds: critical temperatures T_c as a function of NPs average diameter. Blue circles: onset temperature for the catalytic activity of NPs without additional phosphine. The blue area suggests the activity domain for the NPs without additional phosphine. Green arrows indicate the observed enhancement. The green area suggests the region for the enhancement brought by the presence of P^nBu_3 (0.2 equiv.). (B - D) Proposed structures for the active surface. (B) Electronic effect of a nearby phosphine on H_2 activation. (C) Possible NanoFLP with a nickel-phosphine active site. (D) Possible activation of the alkyne by the phosphine prior to the interaction with the surface.

At this stage, it was not possible to determine the precise mechanism of the reaction. Yet, we would like to explain the strong influence of the phosphine steric hindrance and donating capability on the conversion. We can propose several hypotheses, some of them which may collectively be responsible for the enhancement effect observed in this work. In all cases, the presence of phosphide species as surface sites may be responsible for a modified interaction with the phosphine, H_2, and phenylacetylene. As a first proposal, the phosphine may affect the

electronic properties of the surface through its donating character. Schematically, the substrates (H_2 and phenylacetylene) would be adsorbed nearby a phosphine-coordinated surface site, as suggested on Figure 5B, as long as the steric hindrance of the phosphine (or a too high ligand density) does not prevent this. The nature of the phosphine would influence the density of states of the nickel surface nearby. In such a case, we might have expected some correlation of the Hammett parameter of the alkyne on the conversion, and this was not observed. While this does not suffice to disqualify this mechanism, we believe that this lowers the likeliness of this first proposal.

Another proposal is that the active site comprised both the phosphine and a surface Ni atom, in which case there may be a concerted activation of H_2 as one of the transition states (Figure 5C). Such transition state was identified by DFT on gold surfaces.[26,45] The alkyne moiety may also be the one involved in a similar transition state. Steric hindrance of the phosphine would matter as it would influence the ligand surface density and the equilibrium between coordinated phosphine and solvated phosphine. Bulky enough phosphine, in a situation where the surface is crowded by an excess of free phosphine in solution, would experience a frustrated Lewis interaction with the Ni surface, with possibly an elongated P–Ni distance. This would create a reactive pocket, *i.e.* an active site to enable H_2 capture and activation. On the other hand, the donating character of the phosphine would influence the activation of the H–H, C–H and/or C–C bonds of the substrates, as was found for the purely molecular frustrated Lewis pairs in organocatalysis.[46] A too strong interaction would lead to surface site poisoning, while a too bulky phosphine would not be able to approach the surface, because of steric repulsion with native ligands (long-chain amines and phosphines). Lastly, an activation of the phenylacetylene in solution by the phosphine (Figure 5D), resulting in a more active

and transient zwitterionic species, may be proposed in line with previous works of homogeneous catalysis,[47,48] although such species was not detected in the present study.

In the framework of FLPs, we expect a significant influence of both parameters with a delicate compromise to be found for each, as already demonstrated for purely molecular FLPs, especially when the FLP is intermolecular,[46] which is the case here. When considering the stereo-electronic map (Figure 2), we observe that only a narrow region shows a high conversion for phenylacetylene. As a consequence, optimized conditions for a given substrate (here, phenylacetylene) may not be valid for another substrate (e.g. diphenylacetylene). Moreover, this may explain why there is little correlation between the Hammett parameter of the *para*-substituted alkynes and the conversion: a strong sensitivity to the substrate bulkiness is likely and may overcome the electronic effect. In our opinion, both arguments emphasize the likeliness of the NanoFLP proposal.

Nevertheless, the current data do not allow discarding one or the other proposal, as several effects may even exist simultaneously. We strongly believe that computational chemistry methods may help in evaluating the question from an energetic point of view, to be matched with the phosphine-induced lowering of the reaction temperature, which is the main experimental finding of the present work.

3. Conclusion

In this article, we showed that phosphines may be used to lower the onset temperature of phenylacetylene hydrogenation by nickel nanoparticles. This effect stands in contrast with the usual role of these ligands, which is to decrease the activity while increasing the selectivity for styrene. The enhancement observed here is available (i) under a specific set of operating conditions, and (ii) only with adequate phosphines:

(i) We focused on the temperature region corresponding to the onset of the activity of the nickel nanocatalysts under mild reaction conditions (7 bars of H_2), *i.e.* between 40 to 80 °C: in this domain, the addition of P^nBu_3 to the colloidal suspension lowered the onset temperature by 10 to 20 °C, depending on the nanoparticle average diameter. Moreover, the enhancement was stronger when the phosphine was introduced at more than 1 equiv. *vs*. the nickel surface atoms.

(ii) We used a stereo-electronic map to rationalize the ability of 10 phosphines to induce this effect: this allowed us to delineate a region in terms of donating character and bulkiness of the phosphine that was suitable for the reaction. Moderately hindered and fairly donating P^nBu_3 and P^iBu_3 were the most adequate for phenylacetylene hydrogenation.

While we do not expect a practical application of these findings for the hydrogenation of phenylacetylene, its derivatives and other terminal alkynes, which is already a well-mastered process, they allowed us to illustrate the possible formation of a NanoFLP as an active catalytic species. By comparison with the successes of molecular FLPs in organocatalysis, this finding may be an entry point for more challenging reactions such as CO_2 reduction by colloidal metal nanoparticles under mild operating conditions.

Experimental section

Hydrogenation of phenylacetylene. In the glovebox, 50 mL Büchi glass batch reactor was charged with phenylacetylene (1 equiv., 1 mmol, 110 µL), a catalytic amount of Ni NPs (0.1 equiv., 5.87 mg), tri-*n*-butylphosphine (0.2 equiv., 50 µL) and toluene (2 mL). The autoclave was then pressurized with hydrogen (7 bar) and kept under stirring in an oil bath at 60 °C for 16 hours. Once the reactor has cooled down and the hydrogen pressure has been released, the

reaction mixture was then filtrated. NMR tubes were prepared by diluting a drop of the filtrate in $CDCl_3$.

Supporting Information

Reagents and general information, characterization techniques, general procedure for the synthesis of the Ni NPs and characterization, details about the hydrogenation of phenylacetylene, post-mortem characterization, estimation of ligand vs surface metal ratio, complementary catalysis data.

Author contributions

K. A. and A. R. conducted the nanocatalyst syntheses and characterizations. A. R. performed preliminary catalytic tests and K. A. conducted the detailed catalytic study. K. A., A. R. and S. C. performed the data treatment. K. A., A. R. and S. C. conceived the project and co-wrote the manuscript, S. C. spearheading it. All authors approved the final version of the manuscript.

Acknowledgements

This project has received funding from the European Research Council (ERC) under the European Union's Horizon 2020 research and innovation program (grant agreement No 758480). Sorbonne Université and CNRS are acknowledged for support. Antoine Miche and Sandra Casale (Sorbonne Université, CNRS, Fédération de Chimie et Matériaux de Paris-Centre, LRS) are respectively acknowledged for the XPS measurements and HRTEM acquisitions.

References

(1) Refaat, Z.; Saied, M. El; Naga, A. O. A. El; Shaban, S. A.; Hassan, H. B.; Shehata, M. R.; Kady, F. Y. El. Efficient CO2 Methanation Using Nickel Nanoparticles Supported Mesoporous Carbon Nitride Catalysts. *Sci Rep* **2023**, *13* (1), 4855. https://doi.org/10.1038/s41598-023-31958-1.

(2) Baudouin, D.; Rodemerck, U.; Krumeich, F.; Mallmann, A. de; Szeto, K. C.; Ménard, H.; Veyre, L.; Candy, J.-P.; Webb, P. B.; Thieuleux, C.; Copéret, C. Particle Size Effect in the Low Temperature Reforming of Methane by Carbon Dioxide on Silica-Supported Ni Nanoparticles. *J Catal* **2013**, *297*, 27–34. https://doi.org/10.1016/j.jcat.2012.09.011.

(3) Shimizu, K.; Imaiida, N.; Kon, K.; Hakim Siddiki, S. M. A.; Satsuma, A. Heterogeneous Ni Catalysts for N-Alkylation of Amines with Alcohols. *ACS Catal* **2013**, *3* (5), 998–1005. https://doi.org/10.1021/cs4001267.

(4) Zhang, P.; Yu, C.; Fan, X.; Wang, X.; Ling, Z.; Wang, Z.; Qiu, J. Magnetically Recoverable Ni/C Catalysts with Hierarchical Structure and High-Stability for Selective Hydrogenation of Nitroarenes. *Physical Chemistry Chemical Physics* **2015**, *17* (1), 145–150. https://doi.org/10.1039/C4CP03978E.

(5) Osawa, T.; Kizawa, T.; Lee, I.-Y. S.; Ikeda, S.; Kitamura, T.; Inoue, Y.; Borovkov, V. Durability Enhancement of Chirally Modified Metallic Nickel Catalysts for Enantioselective Hydrogenation. *Catal Commun* **2011**, *15* (1), 15–17. https://doi.org/10.1016/j.catcom.2011.08.006.

(6) Ma, Z.; Chandrashekhar, V. G.; Zhou, B.; Alenad, A. M.; Rockstroh, N.; Bartling, S.; Beller, M.; Jagadeesh, R. V. Stable and Reusable Ni-Based Nanoparticles for General

and Selective Hydrogenation of Nitriles to Amines. *Chem Sci* **2022**, *13* (36), 10914–10922. https://doi.org/10.1039/D2SC02961H.

(7) Losch, P.; Huang, W.; Goodman, E. D.; Wrasman, C. J.; Holm, A.; Riscoe, A. R.; Schwalbe, J. A.; Cargnello, M. Colloidal Nanocrystals for Heterogeneous Catalysis. *Nano Today* **2019**, *24*, 15–47. https://doi.org/10.1016/j.nantod.2018.12.002.

(8) Quinson, J.; Neumann, S.; Wannmacher, T.; Kacenauskaite, L.; Inaba, M.; Bucher, J.; Bizzotto, F.; Simonsen, S. B.; Theil Kuhn, L.; Bujak, D.; Zana, A.; Arenz, M.; Kunz, S. Colloids for Catalysts: A Concept for the Preparation of Superior Catalysts of Industrial Relevance. *Angewandte Chemie* **2018**, *130* (38), 12518–12521. https://doi.org/10.1002/ange.201807450.

(9) André, R. F.; Meyniel, L.; Carenco, S. Nickel Carbide (Ni 3 C) Nanoparticles for Catalytic Hydrogenation of Model Compounds in Solvent. *Catal Sci Technol* **2022**, *12* (14), 4572–4583. https://doi.org/10.1039/D2CY00894G.

(10) Jia, C.-J.; Schüth, F. Colloidal Metal Nanoparticles as a Component of Designed Catalyst. *Physical Chemistry Chemical Physics* **2011**, *13* (7), 2457. https://doi.org/10.1039/c0cp02680h.

(11) Raluy, E.; Favier, I.; López-Vinasco, A. M.; Pradel, C.; Martin, E.; Madec, D.; Teuma, E.; Gómez, M. A Smart Palladium Catalyst in Ionic Liquid for Tandem Processes. *Phys Chem Chem Phys* **2011**, *13* (30), 13579–13584. https://doi.org/10.1039/c1cp20619b.

(12) Lara, P.; Philippot, K.; Chaudret, B. Organometallic Ruthenium Nanoparticles: A Comparative Study of the Influence of the Stabilizer on Their Characteristics and Reactivity. *ChemCatChem* **2013**, *5* (1), 28–45. https://doi.org/10.1002/cctc.201200666.

(13) Reina, A.; Favier, I.; Pradel, C.; Gómez, M. Stable Zero-Valent Nickel Nanoparticles in Glycerol: Synthesis and Applications in Selective Hydrogenations. *Adv Synth Catal* **2018**, *360* (18), 3544–3552. https://doi.org/10.1002/adsc.201800786.

(14) Kale, S. S.; Asensio, J. M.; Estrader, M.; Werner, M.; Bordet, A.; Yi, D.; Marbaix, J.; Fazzini, P.-F.; Soulantica, K.; Chaudret, B. Iron Carbide or Iron Carbide/Cobalt Nanoparticles for Magnetically-Induced CO 2 Hydrogenation over Ni/SiRAlOx Catalysts. *Catal Sci Technol* **2019**, *9* (10), 2601–2607. https://doi.org/10.1039/C9CY00437H.

(15) Yan, N.; Yuan, Y.; Dyson, P. J. Nanometallic Chemistry: Deciphering Nanoparticle Catalysis from the Perspective of Organometallic Chemistry and Homogeneous Catalysis. *Dalton Transactions* **2013**, *42* (37), 13294. https://doi.org/10.1039/c3dt51180d.

(16) Kwon, S. G.; Krylova, G.; Sumer, A.; Schwartz, M. M.; Bunel, E. E.; Marshall, C. L.; Chattopadhyay, S.; Lee, B.; Jellinek, J.; Shevchenko, E. V. Capping Ligands as Selectivity Switchers in Hydrogenation Reactions. *Nano Lett* **2012**, *12* (10), 5382–5388. https://doi.org/10.1021/nl3027636.

(17) Ranganath, K. V. S.; Kloesges, J.; Schäfer, A. H.; Glorius, F. Asymmetric Nanocatalysis: N-Heterocyclic Carbenes as Chiral Modifiers of Fe3O4/Pd Nanoparticles. *Angewandte Chemie International Edition* **2010**, *49* (42), 7786–7789. https://doi.org/10.1002/anie.201002782.

(18) Welch, G. C.; Stephan, D. W. Facile Heterolytic Cleavage of Dihydrogen by Phosphines and Boranes. *J Am Chem Soc* **2007**, *129* (7), 1880–1881. https://doi.org/10.1021/ja067961j.

(19) Fiorio, J. L.; López, N.; Rossi, L. M. Gold-Ligand-Catalyzed Selective Hydrogenation of Alkynes into Cis-Alkenes via H2 Heterolytic Activation by Frustrated Lewis Pairs. *ACS Catal* **2017**, *7* (4), 2973–2980. https://doi.org/10.1021/acscatal.6b03441.

(20) Lu, G.; Zhang, P.; Sun, D.; Wang, L.; Zhou, K.; Wang, Z.-X.; Guo, G.-C. Gold Catalyzed Hydrogenations of Small Imines and Nitriles: Enhanced Reactivity of Au Surface toward H 2 via Collaboration with a Lewis Base. *Chem. Sci.* **2014**, *5* (3), 1082–1090. https://doi.org/10.1039/C3SC52851K.

(21) Staiger, L.; Kratky, T.; Günther, S.; Tomanek, O.; Zbořil, R.; Fischer, R. W.; Fischer, R. A.; Cokoja, M. Steric and Electronic Effects of Phosphane Additives on the Catalytic Performance of Colloidal Palladium Nanoparticles in the Semi-Hydrogenation of Alkynes. *ChemCatChem* **2021**, *13* (1), 227–234. https://doi.org/10.1002/cctc.202001121.

(22) Ren, X.; Guo, M.; Li, H.; Li, C.; Yu, L.; Liu, J.; Yang, Q. Microenvironment Engineering of Ruthenium Nanoparticles Incorporated into Silica Nanoreactors for Enhanced Hydrogenations. *Angewandte Chemie International Edition* **2019**, *58* (41), 14483–14488. https://doi.org/10.1002/anie.201908602.

(23) Guo, M.; Li, H.; Ren, Y.; Ren, X.; Yang, Q.; Li, C. Improving Catalytic Hydrogenation Performance of Pd Nanoparticles by Electronic Modulation Using Phosphine Ligands. *ACS Catal* **2018**, *8* (7), 6476–6485. https://doi.org/10.1021/acscatal.8b00872.

(24) Palazzolo, A.; Carenco, S. Phosphines Modulating the Catalytic Silane Activation on Nickel–Cobalt Nanoparticles, Tentatively Attributed to Frustrated Lewis Pairs in a Colloidal Solution. *Chemistry of Materials* **2021**, *33* (19), 7914–7922. https://doi.org/10.1021/acs.chemmater.1c03105.

(25) Ropp, A.; Carenco, S. Influence of the Cobalt Active Site Neighbors in NiCo Nanocatalysts for Phosphine-Assisted Silane Activation. *ChemCatChem* **2023**. https://doi.org/10.1002/cctc.202300400.

(26) Lu, G.; Zhang, P.; Sun, D.; Wang, L.; Zhou, K.; Wang, Z.-X.; Guo, G.-C. Gold Catalyzed Hydrogenations of Small Imines and Nitriles: Enhanced Reactivity of Au Surface toward H 2 via Collaboration with a Lewis Base. *Chem. Sci.* **2014**, *5* (3), 1082–1090. https://doi.org/10.1039/C3SC52851K.

(27) Carenco, S.; Boissière, C.; Nicole, L.; Sanchez, C.; Le Floch, P.; Mézailles, N. Controlled Design of Size-Tunable Monodisperse Nickel Nanoparticles. *Chemistry of Materials* **2010**, *22* (4), 1340–1349. https://doi.org/10.1021/cm902007g.

(28) Carenco, S.; Labouille, S.; Bouchonnet, S.; Boissière, C.; Le Goff, X. F.; Sanchez, C.; Mézailles, N. Revisiting the Molecular Roots of a Ubiquitously Successful Synthesis: Nickel(0) Nanoparticles by Reduction of [Ni(Acetylacetonate) 2]. *Chemistry - A European Journal* **2012**, *18* (44), 14165–14173. https://doi.org/10.1002/chem.201201071.

(29) Carenco, S.; Leyva-Pérez, A.; Concepción, P.; Boissière, C.; Mézailles, N.; Sanchez, C.; Corma, A. Nickel Phosphide Nanocatalysts for the Chemoselective Hydrogenation of Alkynes. *Nano Today* **2012**, *7* (1), 21–28. https://doi.org/10.1016/j.nantod.2011.12.003.

(30) André, R. F.; Palazzolo, A.; Poucin, C.; Ribot, F.; Carenco, S. Phosphine-Catalyzed Activation of Phenylsilane for Benzaldehyde Reduction. *Chempluschem* **2023**. https://doi.org/10.1002/cplu.202300038.

(31) Tolman, C. A. Steric Effects of Phosphorus Ligands in Organometallic Chemistry and Homogeneous Catalysis. *Chem Rev* **1977**, *77* (3), 313–348. https://doi.org/10.1021/cr60307a002.

(32) Fey, N.; Tsipis, A. C.; Harris, S. E.; Harvey, J. N.; Orpen, A. G.; Mansson, R. A. Development of a Ligand Knowledge Base, Part 1: Computational Descriptors for Phosphorus Donor Ligands. *Chemistry - A European Journal* **2006**, *12* (1), 291–302. https://doi.org/10.1002/chem.200500891.

(33) Jover, J.; Cirera, J. Computational Assessment on the Tolman Cone Angles for P-Ligands. *Dalton Transactions* **2019**, *48* (40), 15036–15048. https://doi.org/10.1039/C9DT02876E.

(34) Ropp, A.; André, R. F.; Carenco, S. Phosphine-Enhanced Semi-Hydrogenation of Phenylacetylene by Cobalt Phosphide Nano-Urchins. *Chempluschem* **2023**, *88* (11). https://doi.org/10.1002/cplu.202300469.

(35) Ballesteros-Soberanas, J.; Bilanin, C.; Leyva-Pérez, A. Parametrization of Catalytic Organic Reactions with Convex Hammett Plots. *ACS Organic & Inorganic Au* **2023**, *3* (1), 13–18. https://doi.org/10.1021/acsorginorgau.2c00050.

(36) de los Bernardos, M. D.; Pérez-Rodríguez, S.; Gual, A.; Claver, C.; Godard, C. Facile Synthesis of NHC-Stabilized Ni Nanoparticles and Their Catalytic Application in the Z-Selective Hydrogenation of Alkynes. *Chemical Communications* **2017**, *53* (56), 7894–7897. https://doi.org/10.1039/C7CC01779K.

(37) López-Vinasco, A. M.; Martínez-Prieto, L. M.; Asensio, J. M.; Lecante, P.; Chaudret, B.; Cámpora, J.; van Leeuwen, P. W. N. M. Novel Nickel Nanoparticles Stabilized by

Imidazolium-Amidinate Ligands for Selective Hydrogenation of Alkynes. *Catal Sci Technol* **2020**, *10* (2), 342–350. https://doi.org/10.1039/C9CY02172H.

(38) Ballesteros-Soberanas, J.; Leyva-Pérez, A. Electron-Poor Phosphines Enable the Selective Semihydrogenation Reaction of Alkynes with Pd on Carbon Catalysts. *J Phys Chem Lett* **2023**, *14* (4), 965–970. https://doi.org/10.1021/acs.jpclett.2c03428.

(39) Kwon, S. G.; Krylova, G.; Sumer, A.; Schwartz, M. M.; Bunel, E. E.; Marshall, C. L.; Chattopadhyay, S.; Lee, B.; Jellinek, J.; Shevchenko, E. V. Capping Ligands as Selectivity Switchers in Hydrogenation Reactions. *Nano Lett* **2012**, *12* (10), 5382–5388. https://doi.org/10.1021/nl3027636.

(40) Tuxen, A.; Carenco, S.; Chintapalli, M.; Chuang, C.-H.; Escudero, C.; Pach, E.; Jiang, P.; Borondics, F.; Beberwyck, B.; Alivisatos, A. P.; Thornton, G.; Pong, W.-F.; Guo, J.; Perez, R.; Besenbacher, F.; Salmeron, M. Size-Dependent Dissociation of Carbon Monoxide on Cobalt Nanoparticles. *J Am Chem Soc* **2013**, *135* (6), 2273–2278. https://doi.org/10.1021/ja3105889.

(41) Moreau, L. M.; Ha, D.-H. H.; Bealing, C. R.; Zhang, H.; Hennig, R. G.; Robinson, R. D. Unintended Phosphorus Doping of Nickel Nanoparticles during Synthesis with TOP: A Discovery through Structural Analysis. *Nano Lett* **2012**, *12* (9), 4530–4539. https://doi.org/10.1021/nl301642g.

(42) Carenco, S.; Liu, Z.; Salmeron, M. The Birth of Nickel Phosphide Catalysts: Monitoring Phosphorus Insertion into Nickel. *ChemCatChem* **2017**, *9* (12), 2318–2323. https://doi.org/10.1002/cctc.201601526.

(43) Carenco, S.; Le Goff, X. F.; Shi, J.; Roiban, L.; Ersen, O.; Boissière, C.; Sanchez, C.; Mézailles, N. Magnetic Core−Shell Nanoparticles from Nanoscale-Induced Phase Segregation. *Chemistry of Materials* **2011**, *23* (8), 2270–2277. https://doi.org/10.1021/cm200575g.

(44) Carenco, S.; Leyva-Pérez, A.; Concepción, P.; Boissière, C.; Mézailles, N.; Sanchez, C.; Corma, A. Nickel Phosphide Nanocatalysts for the Chemoselective Hydrogenation of Alkynes. *Nano Today* **2012**, *7* (1), 21–28. https://doi.org/10.1016/j.nantod.2011.12.003.

(45) Fiorio, J. L.; López, N.; Rossi, L. M. Gold-Ligand-Catalyzed Selective Hydrogenation of Alkynes into Cis-Alkenes via H2 Heterolytic Activation by Frustrated Lewis Pairs. *ACS Catal* **2017**, *7* (4), 2973–2980. https://doi.org/10.1021/acscatal.6b03441.

(46) Scott, D. J.; Fuchter, M. J.; Ashley, A. E. Designing Effective 'Frustrated Lewis Pair' Hydrogenation Catalysts. *Chem Soc Rev* **2017**, *46* (19), 5689–5700. https://doi.org/10.1039/C7CS00154A.

(47) Fan, Y. C.; Kwon, O. Advances in Nucleophilic Phosphine Catalysis of Alkenes, Allenes, Alkynes, and MBHADs. *Chemical Communications* **2013**, *49* (99), 11588. https://doi.org/10.1039/c3cc47368f.

(48) Pierce, B. M.; Simpson, B. F.; Ferguson, K. H.; Whittaker, R. E. Phosphine-Mediated Partial Reduction of Alkynes to Form Both (*E*)- and (*Z*)-Alkenes. *Org Biomol Chem* **2018**, *16* (36), 6659–6662. https://doi.org/10.1039/C8OB01848K.

Table of Content Entry